Interfacially engineered oxygen octahedral rotations and their impact on strain relief in coherently grown SrRuO_{3} films

Daisuke Kan, Yusuke Wakabayashi, Hiroo Tajiri, and Yuichi Shimakawa

Phys. Rev. B **94**, 024112 — Published 15 July 2016

DOI: 10.1103/PhysRevB.94.024112

Interfacially engineered oxygen octahedral rotations and their impact on strain relief in coherently grown $SrRuO_3$ films

Daisuke Kan[1*], Yusuke Wakabayashi[2], Hiroo Tajiri[3] and Yuichi Shimakawa[1,4]

[1]*Institute for Chemical Research, Kyoto University, Uji, Kyoto 611-0011, Japan*

[2]*Division of Materials Physics, Graduate School of Engineering Science, Osaka University, Toyonaka 560-8531, Japan*

[3]*Japan Synchrotron Radiation Research Institute, SPring-8, Sayo, Hyogo 679-5198, Japan*

[4]*Japan Science and Technology Agency, CREST, Uji, Kyoto 611-0011, Japan*

*E-mail: dkan@scl.kyoto-u.ac.jp

Abstract

We report synchrotron X-ray diffraction investigations of interfacially engineered oxygen octahedral rotations and their impact on strain relief in perovskite $SrRuO_3$ films. We show that octahedral rotations with distinct patterns and magnitudes can be accommodated into coherently-grown films. The $SrRuO_3$ film grown directly on the $GdScO_3$ substrate has the RuO_6 octahedral rotation with the $a^-b^+c^-$ pattern in the Glazer notation and the rotation angles of $\alpha_{rot} = 6.6 \pm 0.2°$, $\beta_{rot} = 5.5 \pm 0.2°$ and $\gamma_{rot} = 3.6 \pm 0.2°$. On the other hand, when a 1-nm-thick $BaTiO_3$ layer without TiO_6 rotations is inserted between the $SrRuO_3$ and $GdScO_3$, the $SrRuO_3$ has the RuO_6 rotation with $a^-b^0c^+$ and $\alpha_{rot} = 5.6 \pm 0.8°$ and $\gamma_{rot} = 3.6 \pm 0.8°$. These results indicate that there are some degrees of freedom in the octahedral rotations accommodated in $SrRuO_3$ depending on the interface structure and that the γ_{rot} rotations play the important roles in the film's structural properties when the rotation about the $[010]_{pc}$ axis is blocked. We also found that the strain relief in the film is influenced by the interfacially engineered octahedral rotations. The interfacial $BaTiO_3$ layer results in the in-plane periodic lattice modulation in the t-SRO film, allowing for the anisotropic relief of the substrate-induced strain. The results highlight the importance of the interface structure as a factor determining not only octahedral rotations in coherently-grown SRO films but also the strain reliefs in them.

1. Introduction

The various structural and physical properties of transition metal oxides are due in part to the flexibility of the oxygen coordination environments surrounding transition metals. Perovskite oxides consist of three-dimensional networks of corner-shared oxygen octahedra, and various patterns of octahedral rotations (or tilts) characterizing the oxygen coordination environment can be accommodated into the lattice[1,2,3]. Because the octahedral rotations lead to some changes in the M-O-M (M: transition metal) bond lengths and angles, and thus modifications in hybridizations between transition metal 3*d* and oxygen 2*p* orbitals, they are expected to influence structural and physical properties. Recently it has been shown that oxygen octahedral rotations (or oxygen coordination environments) in heterostructured oxides differ from those in bulk oxides, leading to fascinating properties[4,5,6,7,8,9]. It is thus indispensable to understand how the octahedral rotations are accommodated and how they influence structural and physical properties of oxide heterostructures, although the small scattering amplitude of the oxygen atom make it difficult to determine the atomic position precisely.

Our previous studies based on lab-source X-ray diffraction and annular-bright-field (ABF) scanning transmission electron microscopy (STEM) observations[10,11,12] showed that perovskite strontium ruthenate $SrRuO_3$ (SRO) thin films epitaxially grown on $GdScO_3$ (GSO) substrates have

two different structures with distinct oxygen coordination environments surrounding the Ru: one is a monoclinic structure (referred hereafter to as m-SRO) with RuO_6 oxygen octahedra tilted in the out-of-plane direction, and the other is a tetragonal structure (t-SRO) with the tilts strongly suppressed. The SRO film structure can be engineered by changing the heterointerface structure without changing the film thickness (so-called interface engineering) [13,14]. The m-SRO is obtained by depositing SRO directly on the GSO substrate, which forms the interfacial connection between the tilted RuO_6 and ScO_6 octahedra. On the other hand, the t-SRO film is obtained by inserting a few-unit-cells-thick layer of a different oxide ($Ca_{0.5}Sr_{0.5}TiO_3$[12] and $BaTiO_3$[13,14] for example) between SRO and GSO. An inserted $Ca_{0.5}Sr_{0.5}TiO_3$[12] or $BaTiO_3$ (BTO) layer[13,14] leads to the formation of the octahedral connection between the non-tilted RuO_6 and TiO_6 and, as a result, stabilizes the t-SRO films. It is also worthwhile mentioning that the RuO_6 tilts have a close correlation with a magnetic anisotropy of SRO, highlighting the importance of the octahedral tilt (or rotation) as a parameter controlling both structural and physical properties. It is thus important to fully identify the pattern and the magnitude of the octahedral rotations in the SRO films in three dimension and to see how they are modified by the interface engineering. Because the octahedral rotations are in principle characterized by three-dimensional displacements of oxygen from the cubic face-centered position, obtaining two-dimensional oxygen positions projected on a given lattice plane from (S)TEM observations, which basically provides information on the octahedral rotations about only the

observing direction, is not enough to fully identify octahedral rotations accommodated in films[11,12,15,16,17,18].

In this study we used synchrotron X-ray diffraction to fully identify oxygen octahedral rotations in m- and t-SRO films grown on GSO substrates and to see how they are influenced by the heterointerface structures. Quantitative analysis of the diffraction intensity enables one to determine three-dimensional atomic positions of all constituent elements including oxygen, and obtain information about the octahedral rotations in the films[5,7,19,20,21,22,23,24,25,26]. Bulk orthorhombic SRO and GSO both have the rotation pattern described as $a^{-}b^{+}a^{-}$ in the Glazer notation[1,3] while SRO has the smaller rotation angles (α_{rot} ~ 6.6° and β_{rot} ~ 6.2°) than GSO (α_{rot} ~ 14° and β_{rot} ~ 12°). The letters '*a*', '*b*' and '*c*' in the rotation pattern represent the rotation angles about the $[100]_{pc}$ (α_{rot}), $[010]_{pc}$ (β_{rot}), and $[001]_{pc}$ (γ_{rot}) axes, respectively (The subscript pc denotes the pseudocubic perovskite cell). The '+' and '−' signs denote the in-phase and out-of-phase rotations along the axis, respectively, and '0' indicates no rotation. Our quantitative analysis of synchrotron X-ray diffraction measurements revealed that octahedral rotations with distinct patterns and magnitudes, depending on the heterointerface structure, can be accommodated into the coherently-grown $SrRuO_3$ thin films. We also show that the interfacially engineered octahedral rotation affects the relief of the substrate-induced strain in the SRO films.

2. Experimental details

We used pulsed laser deposition to grow m- and t-SRO films ~10 nm thick on $(110)_{ortho}$ $GdScO_3$ (GSO, a_{ortho} = 5.474 Å , b_{ortho} = 5.738 Å, c_{ortho} = 7.925 Å) single crystal substrates (The subscript ortho denotes for the orthorhombic perovskite unit cell). The SRO film's structure was controlled through the interface structure between SRO and GSO[13,14]. The m-SRO film was grown by depositing SRO directly on the substrate (referred to as m-SRO/GSO). The t-SRO, on the other hand, was grown by depositing SRO on the substrate buffered with the 1-nm-thick $BaTiO_3$ (BTO) layer (referred to as t-SRO/BTO/GSO). Lab-source X-ray diffraction including reciprocal space mapping measurements confirmed that there were no secondary phases and that both m- and t-SRO layers were coherently grown on the GSO substrates. We also note that the m- and t-SRO films investigated in this study exhibit metallic conductions down to low temperatures[10,13].

Synchrotron X-ray diffraction measurements of the m-SRO/GSO and t-SRO/BTO/GSO heterostructures at room temperature were carried out at BL13XU in SPring-8[27]. The 20 keV X-ray incident beam with a 0.3 mm × 0.1 mm cross section was used. We recorded and used a total of 39 crystal truncation rods (CTRs) in our structural analysis of the m- and t-SRO films. The diffracted X-rays were collected with a PILATUS detector. The intensity data were obtained by integrating a region of the PILATUS image where the entire signal was detected. The integrated signals were

corrected by subtracting the integrated background signals and by multiplying the remainders by factors based on the footprint, the polarization of the incident beam, and the Lorentz factor[28]. We used the reciprocal lattice unit based on pseudocubic perovskite lattice constants a_{pc} b_{pc}, and c_{pc} along the $[100]_{pc}$, $[010]_{pc}$ and $[001]_{pc}$ directions, the calculation of which was based on the primitive cell of the orthorhombic GSO substrate (approximately $\sqrt{2}a_{pc} \times \sqrt{2}a_{pc} \times 2a_{pc}$). The lattice parameters of the nonprimitive cell of the substrate are a_{pc} = 3.965 (= 7.93/2) Å , b_{pc} = 3.964 (= 7.925/2) Å, c_{pc} = 3.965 (=a_{pc}) Å and β_{pc} = 92.7º. The axes for a_{pc}, b_{pc} and, c_{pc} are parallel to the $[1\bar{1}0]_{ortho}$, $[001]_{ortho}$, and $[110]_{ortho}$ directions of the orthorhombic cell of GSO, respectively.

3. Results and discussion

Figure 1 shows (00*L*) profiles for the m-SRO/GSO and t-SRO/BTO/GSO heterostructures. In addition to the Bragg reflections from the SRO layers seen around $L \sim$ integers, thickness fringes are clearly seen in the entire measuring region up to $L \sim 2.5$, which ensures high uniformity and sharp interfaces of the fabricated heterostructures.

To evaluate RuO_6 octahedral rotations in the m- and t-SRO films, we focused on half-order Bragg reflections which are originated from the doubling of the pseudocubic cell due to the octahedral rotations. It is known[1,2] that the in-phase rotations ('+' rotations) result in the doubling of

the pseudocubic unit cell along the direction normal to the rotation axis, therefore giving rise to half-order reflections that are indexed with one of *H*, *K* and *L* integers and the rests half-integers. On the other hand, the out-of-phase rotations ('−' rotations) double the pseudocubic unit cell along the all axes and thus produce reflections whose indices consist only of half-integers. Figure 2 shows the (1/2 3/2 *L*), (−1/2 3/2 *L*) (−1/2 1 *L*) and (−1 1/2 *L*) profiles for the m-SRO/GSO heterostructures. We note that because the reciprocal lattice unit was determined based on the GSO's orthorhombic structure, the (1/2 3/2 *L*) and (−1/2 3/2 *L*) profiles are not equivalent each other. Half-order reflections associated with the RuO_6 rotations in the m-SRO layer appear when one of the following conditions is satisfied: (1) *H*, *K* and *L* are half-integers, and $K \neq L$, and (2) *H*, *K* and *L* are half-integers, and $H \neq K$, and (3) *H* and *L* are half-integers, *K* is integers and $H \neq L$. We note that these behaviors are confirmed for all profiles measured in this study. The (−1 1/2 1) and (−1 1/2 2) m-SRO reflections observed in Fig. 2c are related to Sr displacements[19]. These observations indicate that the RuO_6 octahedral rotations in the m-SRO layer are described either as $a^-b^+a^-$ or $a^-b^+c^-$. Importantly, the (−1/2 3/2 1/2) m-SRO reflection, which would be extinguished when $\alpha_{rot} = \gamma_{rot}$ (or the $a^-b^+a^-$ rotation pattern), is clearly seen, leading to a conclusion that the m-SRO layer has the $a^-b^+c^-$ rotations ($\alpha_{rot} \neq \gamma_{rot}$). The observed in-phase rotation about the $[010]_{pc}$ axis is consistent with the results of our previous cross-sectional STEM observations of the m-SRO/GSO heterostructure[11,13]. Given that the SRO layer suffers from the 1% tensile strain from the GSO

substrate, this rotation pattern can be regarded as a strain-induced derivation from the octahedral rotation in the bulk orthorhombic SRO ($a^-b^+a^-$). It is also important to point out that the GSO substrate has the ScO_6 rotation with the $a^-b^+a^-$ pattern, which is the same as that of the bulk orthorhombic SRO. In fact, all m-SRO reflections except the (−1/2 3/2 1/2) one are seen associated with those from the GSO substrate (see Fig. 2 for example). This provides experimental evidence that the $a^-b^+c^-$ rotations in the m-SRO film are primarily stabilized by the propagation of the octahedral rotation about the in-plane directions from the substrate.

We observed a different set of half-order reflections for the t-SRO/BTO/GSO heterostructure whose (1/2 3/2 *L*), (−1/2 3/2 *L*), (−1/2 1 *L*), and (−1 1/2 *L*) profiles are shown in Figure 3. The conditions for the half-order reflections due to the RuO_6 rotations are (1) *H*, *K* and *L* are half-integers and $K \neq L$, and (2) *H* and *K* are half-integers, $H \neq K$, and *L* is integers. The observations indicate that the t-SRO layer has the out-of-phase and in-phase rotations about the $[100]_{pc}$ and $[001]_{pc}$ axes, respectively. There are no reflections resulting from neither in-phase nor out-of-phase rotations about the $[010]_{pc}$ axis (Fig. 3b). The rotations in the t-SRO films can therefore be described as $a^-b^0c^+$. No rotations about the $[010]_{pc}$ axis for t-SRO are in close agreements with the results of our cross-sectional ABF-STEM observations of the t-SRO layer that the RuO_6 rotation about the $[010]_{pc}$ axis is negligibly small and the Ru-O-Ru bond angle projected on the $(010)_{pc}$ plane is 178° [13,14]. These results imply that the insertion of the BTO layer at the interface results in the

change in the SRO's unit cell from $\sqrt{2}a_{pc} \times \sqrt{2}a_{pc} \times 2a_{pc}$ for m-SRO to $2a_{pc} \times 2a_{pc} \times 2a_{pc}$ for t-SRO[2,3].

It has been shown[10,13,14] that the SRO films grown on the GSO substrates have the uniaxial magnetic anisotropy and that the direction of the magnetic easy axis depends on the films' structure. The magnetic moment for the m-SRO layer points in the direction tilted by 45º with respect to the out-of-plane direction while the t-SRO layer has the in-plane magnetization pointing in the $[100]_{pc}$ direction (parallel to the $[1\text{-}10]_{ortho}$ direction of the substrate). Based on the obtained unit cells of the SRO layers, the magnetic moments of the m- and t-SRO layers are found to be parallel to the *a* axis of their unit cells, which explains the strong influence of the interface structure on the magnetocrystalline effect of the SRO film[10,13,14].It is also noted that although the BTO layer inserted at SRO/GSO interface[13,14] blocks the substrate-induced propagation of the octahedral rotation and consequently the rotation about the $[010]_{pc}$ axis disappears, the rotation about the $[100]_{pc}$ axis is still seen. This implies that the presence of the in-phase ('+') rotation about the $[010]_{pc}$ axis is strongly dependent on the heterointerface structure including the inserted BTO layer. On the other hand, the out-of-phase ('−') rotation along the $[100]_{pc}$ axis is intrinsically present in the SRO coherently grown on the GSO substrate, regardless of the BTO layer insertion (or the interface structure). Given that in SRO the 4*d* t_{2g} orbitals are partially occupied and their electron occupations influence orbital magnetic moments[29], which affects the magnetic anisotropy through the spin-orbit interaction, the

octahedral rotation about the $[010]_{pc}$ axis plays a crucial role in electron occupations in the t_{2g} orbitals. For m-SRO whose easy axis pointes in the direction at 45º from the surface normal, the orbital magnetic moments should have a component along the surface normal, which is contributed from the d_{yz} and d_{zx} orbitals. Therefore the '+' rotation about the $[010]_{pc}$ axis probably results in preferential occupations of d_{yz} and d_{zx} orbitals, stabilizing the m-SRO's uniaxial magnetic anisotropy. For t-SRO with in-plane magnetization, the orbital magnetic moment should have only an in-plane component and should result from the d_{xy} orbital. This suggests that no rotation about the $[010]_{pc}$ axis due to the interfacial BTO layer lead to preferential occupations in the d_{xy} orbital, which results in the in-plane uniaxial magnetic anisotropy of t-SRO.

To determine detailed structural parameters including rotation angles in the m- and t-SRO films, we calculated half-order reflection intensities from hypothetical heterostructure models and compared them to the observed values. Because of the ScO_6 rotations in GSO, the substrate has non-negligible contributions to the observed half-order reflection intensity. Reflection intensities from the hypothetical models consisting of SRO and GSO were calculated. Details of our calculations are given in Ref. 30. It should be also mentioned that as seen from the observed diffraction profiles (Fig. 2c), the *A*-site Sr displacements associated with the RuO_6 rotations were taken into account in our calculations. Relevant structural parameters for the m- and t-SRO films, determined from the model calculations, are summarized in Table I, and the calculated diffraction

profiles are presented in Figs 1, 2 and 3, where one sees that the observed diffraction profiles are well reproduced. In Figure 4 are shown schematic drawings of the RuO_6 octahedra in the m- and t-SRO films based on the determined parameters. For the m-SRO film with the $a^-b^+c^-$ rotations, the rotation angles are determined to be $\alpha_{rot} = 6.6 \pm 0.2°$, $\beta_{rot} = 5.5 \pm 0.2°$ and $\gamma_{rot} = 3.6 \pm 0.2°$, and the corresponding Ru-O-Ru bond angle projected on the $(010)_{pc}$ plane is 169.2°, which is in close agreement with the bond angle obtained from the cross-sectional ABF-STEM observations (168°). The results reveal that the γ_{rot} rotations, which are not detectable by ABF-STEM, are largely reduced while the α_{rot} and β_{rot} rotations are comparable to those in the bulk SRO. The reduction in the γ_{rot} rotation can be attributed to the substrate-induced tensile strain, which elongates the in-plane bond length between the Ru and the oxygen and consequently suppresses in the rotation about the out-of-plane direction. Similar tensile-strain-induced reduction in the γ_{rot} rotations was observed for other perovskite oxides[20]. The out-of-plane bond length, in contrast, is little influenced by the strain. This explains why the RuO_6 rotations about the in-plane $[100]_{pc}$ and $[010]_{pc}$ axes are comparable to the bulk. Consequently Sr displacements comparable to that in the bulk SRO is also present in the m-SRO film[30].

For the t-SRO film with the $a^-b^0c^+$ rotations (no rotation about the $[010]_{pc}$ axis), we obtain $\alpha_{rot} = 5.6 \pm 0.8°$ and $\gamma_{rot} = 3.6 \pm 0.8°$. The rotation angle about the $[100]_{pc}$ axis (α_{rot}) is close to that of the bulk SRO, which provides experimental support that the accommodation of the

out-of-phase rotation is not a result of the insertion of the BTO layer and is intrinsically introduced in the SRO under the tensile strain from the GSO substrate. It is worthwhile mentioning that the high-temperature tetragonal phase of SRO has the out-of-phase rotation with the $a^0a^0c^-$ pattern and that the in-phase rotations are introduced upon the structural phase transition from the tetragonal structure to the low-temperature orthorhombic one in the bulk SRO[31]. In the t-SRO film, the inserted BTO layer prohibits the in-phase rotations about the in-plane axes. This is why the in-phase rotation of t-SRO is introduced about the out-of-plane axis while its magnitude is small (γ_{rot} ~ 3.5º) due to the substrate-induced tensile strain. In fact, the γ_{rot} rotation angle of the t-SRO (3.6 ± 0.8°) is comparable that of m-SRO (3.6 ± 0.2°). This in-phase γ_{rot} rotation plays an important role in releasing the lattice energy accumulated because of the substrate-induced strain.

We also found that the t-SRO film has periodic lattice modulation along the in-plane direction. Figures 5a and 5b present results of *K* and *H* scans around various t-SRO reflections. The diffraction intensities for these scans were collected by a YAP scintillation detector. Besides Bragg reflections from the film layer at $\Delta K = 0$, satellite reflections appear at $\Delta K \sim \pm 0.023$ reciprocal lattice units (r.l.u.). The positions of the satellite reflections are independent of the indexes of the measured Bragg reflections (Fig. 5a). As shown in Fig. 5b, on the other hand, no satellite reflections are evident in the *H* scans. These observations indicate that the t-SRO film lattice is periodically modulated along the $[010]_{pc}$ direction and the period of the modulation is calculated to be 17 nm,

approximately corresponds to 22 t-SRO unit cells (in terms of the $2a_{pc} \times 2a_{pc} \times 2a_{pc}$ cell). It should be pointed out that the observed in-plane lattice modulations in t-SRO is unlikely to arise from possible ferroelectricity in the inserted thin BTO layer because depolarization-induced stripe domains of BTO films under compressive strain would form along the $[110]_{pc}$ direction[32,33], which cannot explain the observed lattice modulation along the $[010]_{pc}$ direction of the t-SRO film. Instead, the lattice modulation in SRO is attributed to anisotropic relief of the substrate-induced strain. Similar in-plane lattice modulations were observed for epitaxial thin films of perovskite oxides[34,35,36]. In the t-SRO film, the in-phase rotation about the $[010]_{pc}$ axis is blocked by the interfacial BTO layer and the γ rotation is suppressed due to the substrate-induced tensile strain, implying that the strain relief due to the octahedral rotation is not large enough to stabilize the t-SRO structural phase without the additional strain relief introduced by the anisotropic lattice modulation. Although our calculation for the hypothetical t-SRO/GSO heterostructure in which Sr displacements expected from the rotation pattern are included does not reproduce the observed half-order reflections, such as (2 0 3/2) and (−2 0 3/2) with the satellite reflections, additional cation displacements along either the $[100]_{pc}$ or $[001]_{pc}$ directions (or along both directions) are the plausible origin of these half-order reflections. We also note that such satellite reflections are not seen in the m-SRO films, highlighting the strong influence of the interfacially engineered octahedral rotation on the strain relief in the SRO films.

4. Summary

We quantitatively evaluated interfacially engineered oxygen octahedral rotations in SRO epitaxial thin films by synchrotron X-ray diffraction. We showed that the monoclinic SRO film directly grown on the GSO substrate has the $a^{-}b^{+}c^{-}$ pattern of RuO_6 rotations with rotation angles of $\alpha_{rot} = 6.6 \pm 0.2°$, $\beta_{rot} = 5.5 \pm 0.2°$ and $\gamma_{rot} = 3.6 \pm 0.2°$. On the other hand, the tetragonal SRO film grown on the BTO-buffered GSO substrate has the rotations with the $a^{-}b^{0}c^{+}$ pattern and $\alpha_{rot} = 5.6 \pm 0.8°$ and $\gamma_{rot} = 3.6 \pm 0.8°$. These results indicate that there are some degrees of freedom in the octahedral rotations accommodated in SRO, which strongly depend on the interface structure between SRO and GSO. We also showed that when the rotation about the $[010]_{pc}$ axis is blocked by inserting the BTO layer, the γ_{rot} rotations, which is not observed by the STEM-based technique, play the important roles in film's structural properties and that the interfacial BTO layer leads to anisotropic strain relaxation associated with the in-plane periodic lattice modulation in the tetragonal SRO film. The results highlight the strong influence of the interfacially engineered octahedral rotation on the strain relief in the coherently-grown SRO films.

Acknowledgements

This work was partially supported by a grant for the Joint Project of Chemical Synthesis Core Research Institutions from the Ministry of Education, Culture, Sports, Science and Technology (MEXT) of Japan. The work was also supported by Japan Science and Technology Agency, CREST. This work was partially supported by JSPS KAKENHI Grant Number 26105008. The x-ray diffraction measurements at SPring-8 were performed with the approval of the Japan Synchrotron Radiation Research Institute (2015A1566 and 2015B1146).

Table I: Structural parameters for the m- and t-SRO films determined from the synchrotron x-ray diffraction profiles and their analysis based on the model calculations. (Details of the analysis are given in Ref. 30). Note that the SRO films are coherently grown on the GSO substrate and the in-plane lattice constants of SRO are fixed to be identical to those of the substrate. For SRO and GSO, the axes for a_{pc}, b_{pc} and, c_{pc} are parallel to the $[1\bar{1}0]_{ortho}$,$[001]_{ortho}$, and $[110]_{ortho}$ directions of the orthorhombic cell, respectively.

	Lattice param.	Symmetry	Rotation pattern	Rotation angle	# of unit cell (Thickness)
m-SRO film (on GSO sub.)	$a_{pc} = a_{GSO\_pc}$ b_{pc} =3.964 ± 0.002 Å $c_{pc} = c_{GSO\_pc}$ β_{pc} = 89.5± 0.1º	$P2_1/m$	$a^-b^+c^-$	α_{rot} = 6.6 ± 0.2º β_{rot} = 5.5 ± 0.2º γ_{rot} = 3.6 ± 0.2º	22 u.c. (~ 9 nm)
t-SRO film (on GSO sub.)	$a_{pc} = a_{GSO\_pc}$ b_{pc} =3.964 ± 0.002 Å	$Ccmm$	$a^-b^0c^+$	α_{rot} = 5.6 ± 0.8º γ_{rot} = 3.6 ± 0.8º	26 u.c. (~ 10 nm)

	$c_{pc} = c_{GSO\_pc}$ $\beta_{pc} = 90^o$				
Bulk SRO (ortho.)	$a_{pc} = 3.930$ Å $b_{pc} = 3.922$ Å $c_{pc} = 3.930$ Å $\beta_{pc} = 89.8^o$	*Pbnm*	$a^-b^+a^-$	$\alpha_{rot} \sim 6.6^o$ $\beta_{rot} \sim 6.2^o$	
Bulk GSO (ortho.)	$a_{pc} = 3.965$ Å $b_{pc} = 3.964$ Å $c_{pc} = 3.965$ Å $\beta_{pc} = 92.7^o$	*Pbnm*	$a^-b^+a^-$	$\alpha_{rot} \sim 14^o$ $\beta_{rot} \sim 12^o$	

Figure captions

Figure 1: Measured and calculated (00*L*) profiles of the m-SRO/GSO (red) and t-SRO/BTO/GSO heterostructures (blue). The calculated profile is colored in green (For details of the calculations, see the main text and Ref. 30). The peaks marked with the asterisk (*) in the profiles are due to multiple scatterings from the GSO substrate.

Figure 2: Measured (red) and calculated (green) (a) (1/2 3/2 *L*) and (−1/2 3/2 *L*), (b) (−1/2 1 *L*) and (c) (−1 1/2 *L*) profiles of the m-SRO/GSO heterostructure.

Figure 3: Measured (blue) and calculated (green) (a) (1/2 3/2 *L*) and (−1/2 3/2 *L*), (b) (−1/2 1 *L*) and (c) (−1 1/2 *L*) profiles (blue) of the t-SRO/BTO/GSO heterostructures.

Figure 4: Schematic drawings of the RuO_6 octahedra in (a) m- and (b) t-SRO films. Sr atoms are omitted for clarity.

Figure 5: (a) *K* and (b) *H* scans taken around various Bragg reflections of the t-SRO films. The

diffraction intensities were measured with a YAP (yttrium aluminum perovskite) scintillation detector.

References

1 A. M. Glazer, Acta Crystallographica Section B **28**, 3384 (1972).

2 A. Glazer, Acta Crystallographica Section A **31**, 756 (1975).

3 P. M. Woodward, Acta Crystallographica Section B **53**, 32 (1997).

4 Y.-M. Kim, A. Kumar, A. Hatt, A. N. Morozovska, A. Tselev, M. D. Biegalski, I. Ivanov, E. A. Eliseev, S. J. Pennycook, J. M. Rondinelli, S. V. Kalinin, and A. Y. Borisevich, Adv. Mater. **25**, 2497 (2013).

5 E. J. Moon, R. Colby, Q. Wang, E. Karapetrova, C. M. Schlepütz, M. R. Fitzsimmons, and S. J. May, Nat Commun **5**, 5710 (2014).

6 B. Rivas-Murias, I. Lucas, P. Jiménez-Cavero, C. Magén, L. Morellón, and F. Rivadulla, Nano Lett. **16**, 1736 (2016).

7 M. D. Biegalski, L. Qiao, Y. Gu, A. Mehta, Q. He, Y. Takamura, A. Borisevich, and L.-Q. Chen, Appl. Phys. Lett. **106**, 162904 (2015).

8 M. D. Biegalski, Y. Takamura, A. Mehta, Z. Gai, S. V. Kalinin, H. Ambaye, V. Lauter, D. Fong, S. T. Pantelides, Y. M. Kim, J. He, A. Borisevich, W. Siemons, and H. M. Christen, Advanced Materials Interfaces **1**, 1400203 (2014).

9 X. Zhai, L. Cheng, Y. Liu, C. M. Schlepütz, S. Dong, H. Li, X. Zhang, S. Chu, L. Zheng, J. Zhang, A. Zhao, H. Hong, A. Bhattacharya, J. N. Eckstein, and C. Zeng, Nat Commun **5** (2014).

10 D. Kan, R. Aso, H. Kurata, and Y. Shimakawa, Adv. Funct. Mater. **23**, 1129 (2013).

11 R. Aso, D. Kan, Y. Shimakawa, and H. Kurata, Scientific reports **3**, 2214 (2013).

[12] D. Kan, R. Aso, R. Sato, M. Haruta, H. Kurata, and Y. Shimakawa, Nat. Mater. **15**, 432 (2016).

[13] R. Aso, D. Kan, Y. Shimakawa, and H. Kurata, Adv. Funct. Mater. **24**, 5177 (2014).

[14] D. Kan, R. Aso, H. Kurata, and Y. Shimakawa, J. Appl. Phys. **115**, 184304 (2014).

[15] A. Y. Borisevich, H. J. Chang, M. Huijben, M. P. Oxley, S. Okamoto, M. K. Niranjan, J. D. Burton, E. Y. Tsymbal, Y. H. Chu, P. Yu, R. Ramesh, S. V. Kalinin, and S. J. Pennycook, Phys. Rev. Lett. **105**, 087204 (2010).

[16] Q. He, R. Ishikawa, A. R. Lupini, L. Qiao, E. J. Moon, O. Ovchinnikov, S. J. May, M. D. Biegalski, and A. Borisevich, ACS Nano **9**, 8412 (2015).

[17] M. O'Sullivan, J. Hadermann, M. S. Dyer, S. Turner, J. Alaria, T. D. Manning, A. M. Abakumov, J. B. Claridge, and M. J. Rosseinsky, Nat Chem **advance online publication** (2016).

[18] C. L. Jia, S. B. Mi, M. Faley, U. Poppe, J. Schubert, and K. Urban, Phys. Rev. B **79**, 081405 (2009).

[19] H. Rotella, U. Lüders, P. E. Janolin, V. H. Dao, D. Chateigner, R. Feyerherm, E. Dudzik, and W. Prellier, Phys. Rev. B **85**, 184101 (2012).

[20] S. J. May, J. W. Kim, J. M. Rondinelli, E. Karapetrova, N. A. Spaldin, A. Bhattacharya, and P. J. Ryan, Phys. Rev. B **82**, 014110 (2010).

[21] T. T. Fister, H. Zhou, Z. Luo, S. S. A. Seo, S. O. Hruszkewycz, D. L. Proffit, J. A. Eastman, P. H. Fuoss, P. M. Baldo, H. N. Lee, and D. D. Fong, APL Materials **2**, 021102 (2014).

[22] R. Yamamoto, C. Bell, Y. Hikita, H. Y. Hwang, H. Nakamura, T. Kimura, and Y. Wakabayashi, Phys. Rev. Lett. **107**, 036104 (2011).

[23] B. Zhang, C.-J. Sun, P. Yang, W. Lu, B. L. Fisher, T. Venkatesan, S. M. Heald, J.-S. Chen, and G. M. Chow, Phys. Rev. B **89**, 195140 (2014).

[24] W. Lu, P. Yang, W. D. Song, G. M. Chow, and J. S. Chen, Phys. Rev. B **88**, 214115 (2013).

[25] A. Vailionis, H. Boschker, Z. Liao, J. R. A. Smit, G. Rijnders, M. Huijben, and G. Koster, Appl. Phys. Lett. **105**, 131906 (2014).

[26] R. L. Johnson-Wilke, D. Marincel, S. Zhu, M. P. Warusawithana, A. Hatt, J. Sayre, K. T. Delaney, R. Engel-Herbert, C. M. Schlepütz, J. W. Kim, V. Gopalan, N. A. Spaldin, D. G. Schlom, P. J. Ryan, and S. Trolier-McKinstry, Phys. Rev. B **88**, 174101 (2013).

[27] O. Sakata, Y. Furukawa, S. Goto, T. Mochizuki, T. Uruga, K. Takeshita, H. Ohashi, T. Ohata, T. Matsushita, S. Takahashi, H. Tajiri, T. Ishikawa, M. Nakamura, M. Ito, K. Sumitani, T. Takahashi, T. Shimura, A. Saito, and M. Takahasi, Surf. Rev. Lett. **10**, 543 (2003).

[28] C. M. Schleputz, R. Herger, P. R. Willmott, B. D. Patterson, O. Bunk, C. Bronnimann, B. Henrich, G. Hulsen, and E. F. Eikenberry, Acta Crystallographica Section A **61**, 418 (2005).

[29] K. Ishigami, K. Yoshimatsu, D. Toyota, M. Takizawa, T. Yoshida, G. Shibata, T. Harano, Y. Takahashi, T. Kadono, V. K. Verma, V. R. Singh, Y. Takeda, T. Okane, Y. Saitoh, H. Yamagami, T. Koide, M. Oshima, H. Kumigashira, and A. Fujimori, Phys. Rev. B **92**, 064402 (2015).

[30] See Supplemental Material at URL for details of our calculations for reflection intensities from the heterostructures.

[31] B. J. Kennedy and B. A. Hunter, Phys. Rev. B **58**, 653 (1998).

[32] D. A. Tenne, P. Turner, J. D. Schmidt, M. Biegalski, Y. L. Li, L. Q. Chen, A. Soukiassian, S. Trolier-McKinstry, D. G. Schlom, X. X. Xi, D. D. Fong, P. H. Fuoss, J. A. Eastman, G. B. Stephenson, C. Thompson, and S. K. Streiffer, Phys. Rev. Lett. **103**, 177601 (2009).

[33] B.-K. Lai, I. Ponomareva, I. A. Kornev, L. Bellaiche, and G. J. Salamo, Phys. Rev. B **75**, 085412 (2007).

[34] U. Gebhardt, N. V. Kasper, A. Vigliante, P. Wochner, H. Dosch, F. S. Razavi, and H. U. Habermeier, Phys. Rev. Lett. **98**, 096101 (2007).

[35] J. E. Boschker, C. Folkman, C. W. Bark, Å. F. Monsen, E. Folven, J. K. Grepstad, E. Wahlström, C. B. Eom, and T. Tybell, Phys. Rev. B **84**, 205418 (2011).

[36] A. Vailionis, H. Boschker, E. Houwman, G. Koster, G. Rijnders, and D. H. A. Blank, Appl. Phys. Lett. **95**, 152508 (2009).

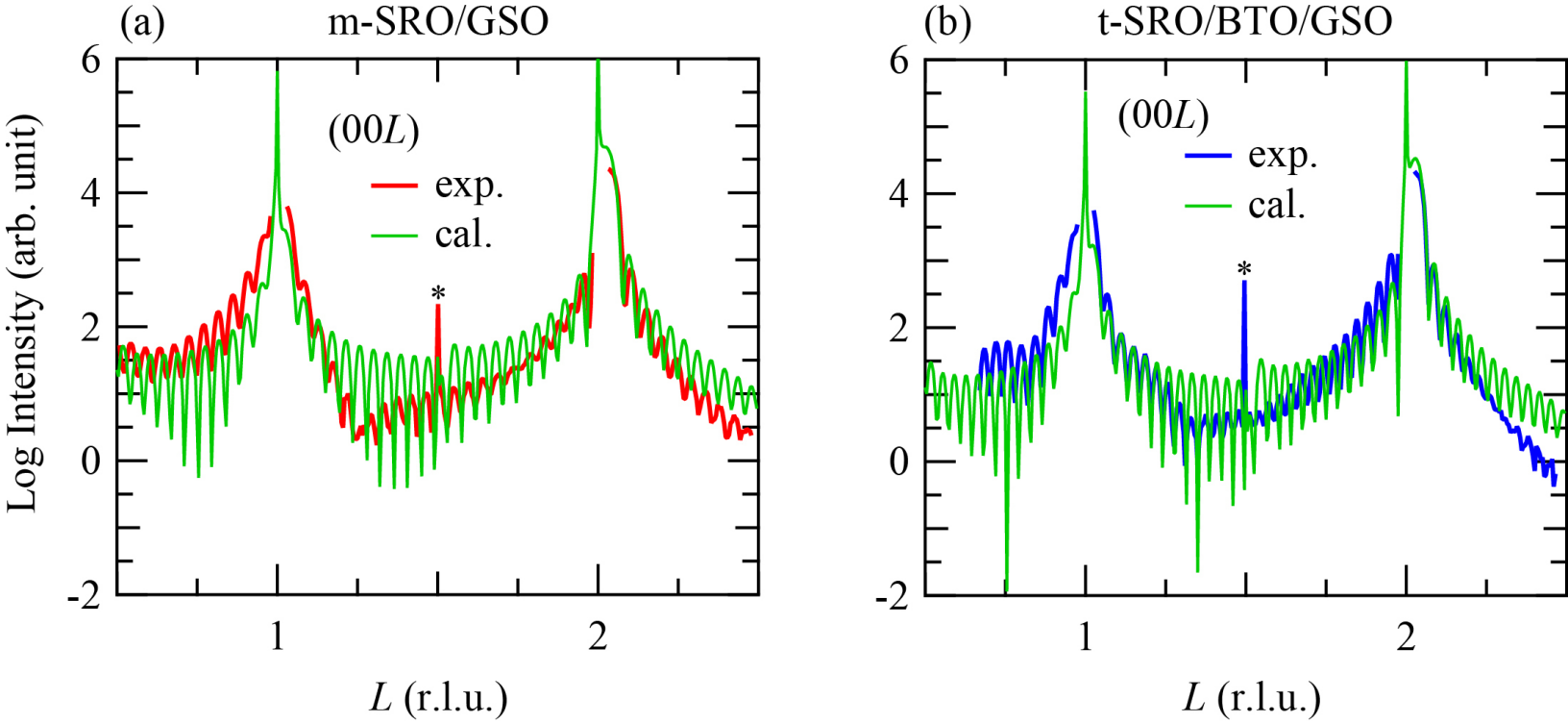
(a)
m-SRO/GSO
(00L)
exp.
cal.
*
Log Intensity (arb. unit)
L (r.l.u.)
(b)
t-SRO/BTO/GSO
(00L)
exp.
cal.
*
L (r.l.u.)

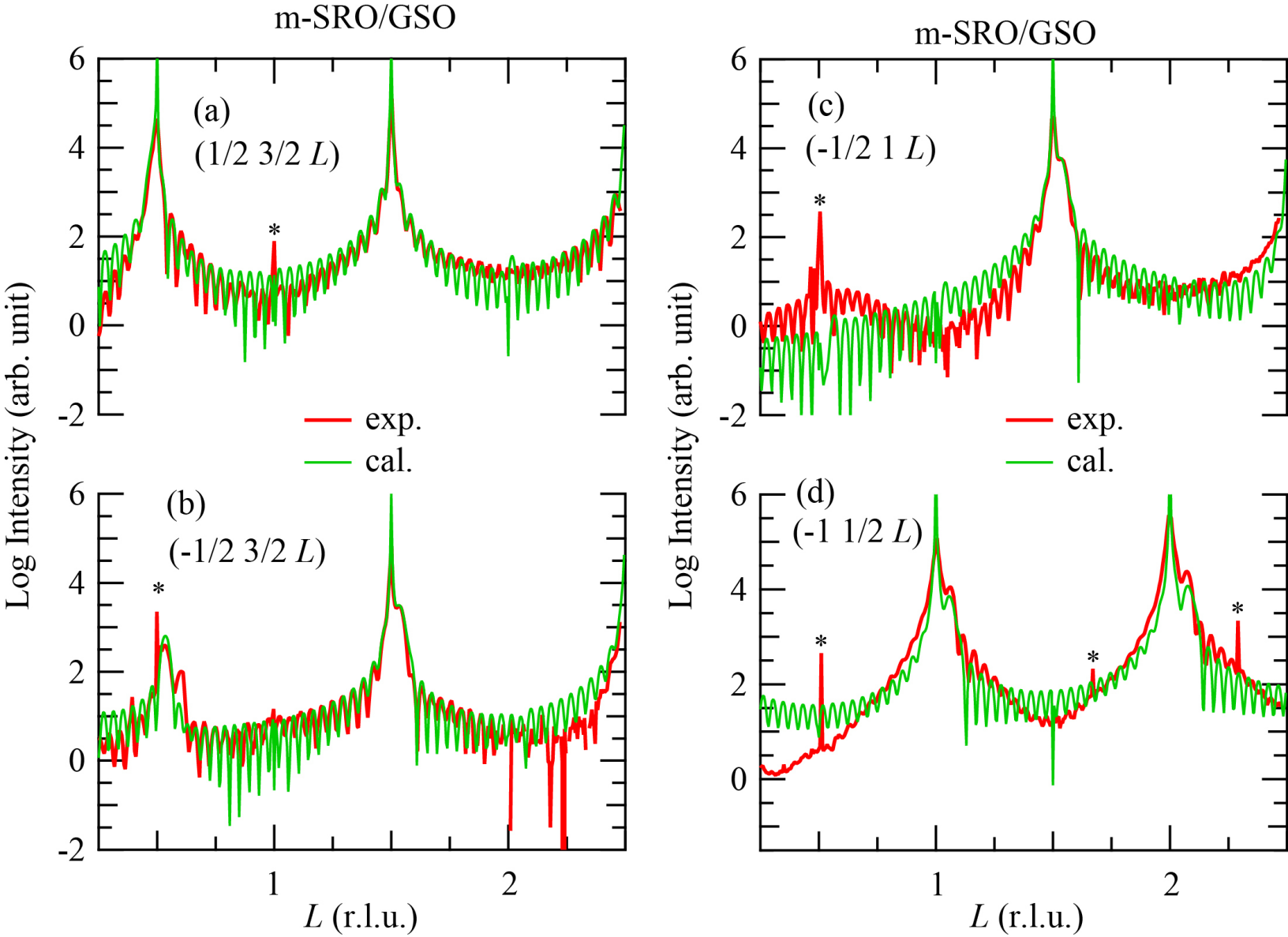
m-SRO/GSO
(a)
(1/2 3/2 L)
exp.
cal.
(b)
(-1/2 3/2 L)
Log Intensity (arb. unit)
L (r.l.u.)
m-SRO/GSO
(c)
(-1/2 1 L)
exp.
cal.
(d)
(-1 1/2 L)
Log Intensity (arb. unit)
L (r.l.u.)

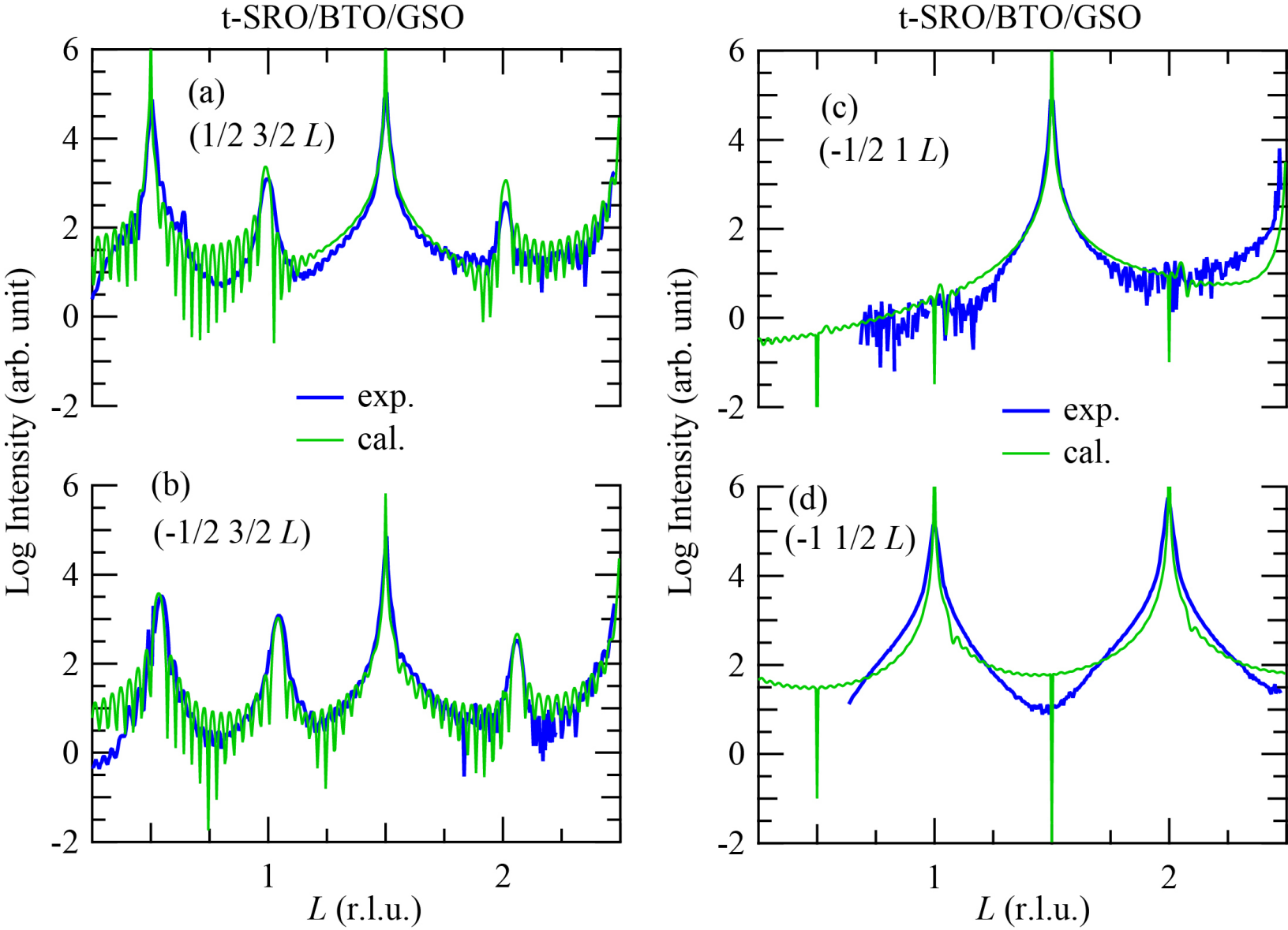
t-SRO/BTO/GSO
t-SRO/BTO/GSO
(a)
(1/2 3/2 L)
(b)
(-1/2 3/2 L)
(c)
(-1/2 1 L)
(d)
(-1 1/2 L)
exp.
cal.
exp.
cal.
Log Intensity (arb. unit)
Log Intensity (arb. unit)
L (r.l.u.)
L (r.l.u.)
6
4
2
0
-2
1
2

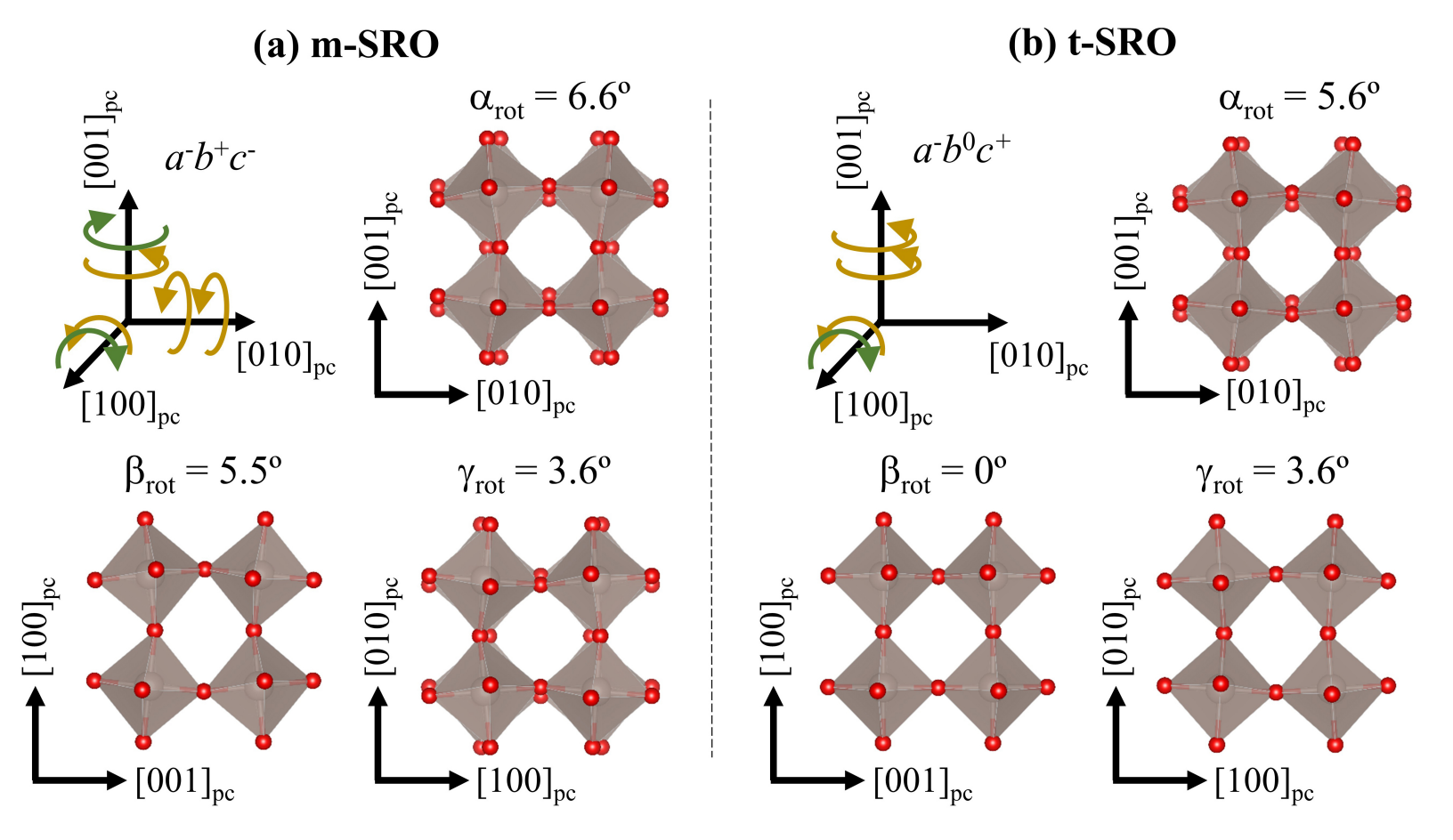
(a) m-SRO
(b) t-SRO
$a^-b^+c^-$
$a^-b^0c^+$
α_{rot} = 6.6°
α_{rot} = 5.6°
β_{rot} = 5.5°
β_{rot} = 0°
γ_{rot} = 3.6°
γ_{rot} = 3.6°
[001]pc
[010]pc
[100]pc

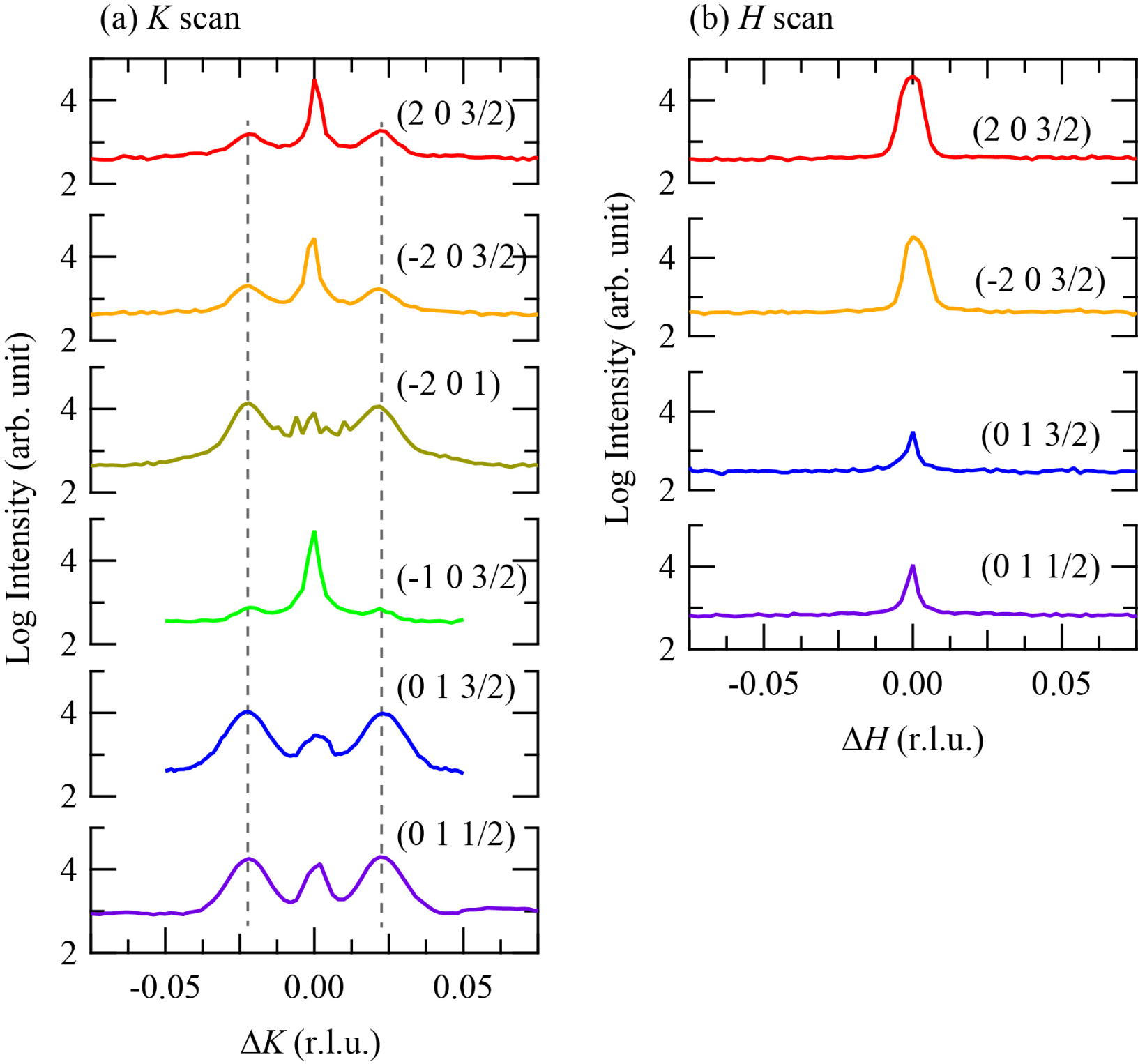
(a) K scan
(b) H scan
(2 0 3/2)
(-2 0 3/2)
(-2 0 1)
(-1 0 3/2)
(0 1 3/2)
(0 1 1/2)
Log Intensity (arb. unit)
ΔK (r.l.u.)
ΔH (r.l.u.)
-0.05
0.00
0.05
2
4